Active Pneumatic Suspension for Future Autonomous Vehicles: Design, Prove of Concept and Hardware-in-the-Loop Simulations

REVIEWED

P. Hedrich*, E. Lenz**, N. Brötz* and P. F. Pelz*

Institut für Fluidsystemtechnik, Technische Universität Darmstadt
Otto-Berndt-Str. 2, D-64287 Darmstadt, Germany*
Fachgebiet Regelungstechnik und Mechatronik, Technische Universität Darmstadt
Landgraf-Georg-Str. 4, D-64283 Darmstadt, Germany**
E-Mail: Peter.Pelz@fst.tu-darmstadt.de

In this article, we present a new concept of an active air spring, which can apply pressure and tension forces independently of its deflection. The active strut mitigates body oscillations and improves the driving comfort making it attractive for autonomous driving to avoid motion sickness. The model of the active air spring system and the controller design are described. Furthermore, the suitability of the actuator concept for use in an active chassis is shown. Finally, we show results of hardware-in-the-loop simulations.

Keywords: active suspension, active air spring, hydraulic actuator, controller design, hardware-in-the-loop
Target audience: mobile hydraulics, pneumatics, hardware-in-the-loop, control

1 Motivation

Experts assume that autonomous driving is the key technology for our future transport system. A major advantage of this technology is that the occupants are able to engage in other activities while driving. In addition, one assumes that passengers will accept longer journeys since driving does not seem to be a loss of time /1/. However, studies have shown that the incidence of kinetosis, i. e. motion sickness, is significantly higher in autonomous driving than in conventional vehicles and one out of ten passengers will suffer from moderate to serious motion sickness often to always /2/. For this reason, the new technology could only be accepted slowly or even rejected. Consequently, it is important to take measures to minimize the incidence of kinetosis during autonomous driving.

Although the phenomenon has been scientifically researched for a long time, it has not been fully understood to date. The three main factors for kinetosis which could be found are (i) a conflict between visual and vestibular inputs, (ii) a loss of control of one's movements and (iii) a reduced ability to anticipate the direction of movement /2/. Decoupling the environment and the driving dynamics is a promising approach to minimize the incidence of motion sickness. Since especially vertical dynamic excitations, i. e. heave, are perceived as particularly disturbing in a low-frequency range from 0.1 Hz to approx. 1 Hz /3/, controlled semi-active or active suspensions can provide a remedy /4/. This could lead to a renaissance of active suspension systems and provide opportunities for new active technologies. In contrast to conventional passive or semi-active systems, active systems have a flexible working area and can, therefore, react to uncertainty during usage, e. g. changing excitations or system parameters. Additionally, active suspension systems can reduce oscillations by applying pressure and tension forces independent of the strut deflection /5/.

These measures will further differentiate the vehicle market. On the one hand, there will be expensive, comfort oriented high-tech vehicles that serve as rolling offices or living rooms and use the above-mentioned technologies to maximise driving comfort. On the other hand, there will be low-cost transport vehicles that meet the requirements for the transport service but are more like small city buses and do not have any emotional appeal nor satisfy high demands for comfort /4/.

2 The TU Darmstadt Active Air Spring

Nowadays, conventional spring dampers are based on mechanical spring elements, or air springs, in combination with hydraulic dampers. The separation of the main functions "load-carrying" and "energy storing" of the air spring is an advantage over mechanical springs. It enables a level control by adapting the mass of the air inside the air spring to its load. This means that the level between the road and the vehicle body can be adjusted, for example, to lower the body when the passengers entering the car or when driving on a motorway for minimizing the drag. In addition, the full suspension travel for rebound and compression can be used. Furthermore, the oscillation behaviour of the system remains approximately the same due to the practically constant natural frequency of the car body. At the same time, it is ensured that all wheels are in close contact with the road. In consequence, this increases the driving safety /6/.

The active air spring is an active spring element based on an air spring that combines the above-mentioned advantages of an active system with those of an air spring. The axial force of the air spring is the product of the load-carrying (pressure effective) area A_L and the pressure difference between the internal pressure of the air spring p and the ambient pressure p_a,

$$F = (p - p_\mathrm{a}) A_\mathrm{L} \,. \tag{1}$$

By differentiating equation (1) and assuming an isentropic state change , which leads to

$$\begin{aligned} \frac{\mathrm{d}F}{F_0} &= \frac{1}{F_0}\left[A_\mathrm{L}\,\mathrm{d}p + (p - p_\mathrm{a})\,\mathrm{d}A_\mathrm{L}\right] \\ &\approx \frac{1}{F_0}\left[A_\mathrm{L}\,\mathrm{d}p + p\,\mathrm{d}A_\mathrm{L}\right] \\ &= -\gamma\,\frac{\mathrm{d}V}{\mathrm{d}z}\,\frac{\mathrm{d}z}{V_0} + \frac{\mathrm{d}m}{m_0} + \frac{\mathrm{d}A_\mathrm{L}}{A_{\mathrm{L}0}}, \end{aligned} \tag{2}$$

different approaches for manipulating the axial force of the air spring become obvious /7/. In equation (2), V denotes the volume of the air spring, z its compression, m the mass of the compressed air and γ the isentropic constant. The first expression on the right side of the last line of equation (2) represents the change in the force due to the compression of the air spring, the second one the influence of the mass of the compressed air (which is relevant for the above-mentioned quasi-static level control) and the last one the influence of the load-carrying area. A linearisation of equation (2) for the working point of the air spring (compression $z = 0$) leads to

$$\frac{\Delta F}{F_0} \approx \gamma\, A_{\mathrm{D}0}\,\frac{\Delta z}{V_0} + \frac{\Delta m}{m_0} + \frac{\Delta A_\mathrm{L}}{A_{\mathrm{L}0}}, \tag{3}$$

with the displacement area of the air spring $A_{\mathrm{D}0} := -\mathrm{d}V/\mathrm{d}z\big|_0$. The resulting total axial force of the air spring is

$$\begin{aligned} F &= F_0 + \Delta F \\ &= F_0 + c\,\Delta z + \frac{p_0 A_{\mathrm{L}0}}{m_0}\,\Delta m + p_0\,\Delta A_{L0}, \end{aligned} \tag{4}$$

with the air spring stiffness $c := \gamma\, p_0 A_{\mathrm{D}0} A_{\mathrm{L}0}/V_0$. Equation (4) illustrates two possibilities for manipulating the axial force independently of the spring deflection: (i) by adjusting the mass of the compressed air m in the air spring or (ii) the load-carrying-area A_L. Due to the compressibility of the air, the adaptation of the air mass at frequencies which are necessary for manipulating the oscillation of the car body or the wheel, approximately 5 Hz and 30 Hz /5, 8/, is impossible. For this reason, adjusting the load-carrying area seems to be the only reasonable approach to actively change the axial force of an air spring.

The load-carrying area of an air spring with the rolling piston radius r_P and the outside guide radius r_O is

$$A_\mathrm{L} \approx \frac{\pi}{4}\,(r_\mathrm{P} + r_\mathrm{O})^2 \,. \tag{5}$$

Our approach is to adjust the load-carrying area by changing the rolling piston radius of the air spring /9/. For this purpose, we developed an air spring piston, which radius can be adjusted hydraulically with four segments. The segments are evenly distributed over the circumference /10, 11/, Figure 1.

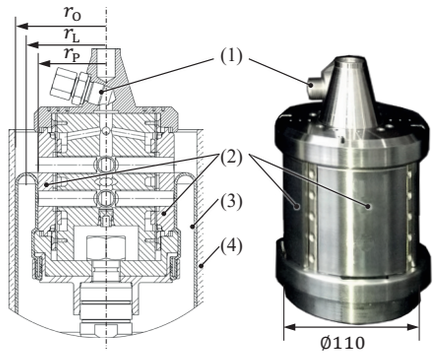

Figure 1: The integrated hydraulic actuator can adjust the radius of the air spring rolling piston r_P during the usage with an edge frequency of 5 Hz, (1) labels the hydraulic connection, (2) the adjustable circle segments of the rolling piston, (3) the air spring bellows and (4) the outside guide of the air spring.

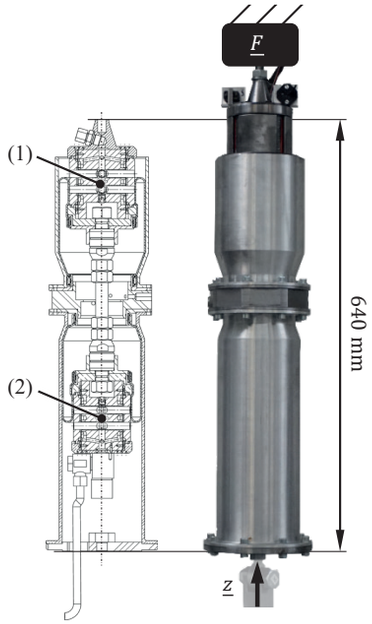

Figure 2: The active air spring with two hydraulically adjustable rolling pistons, (1) and (2).

Table 1: Parameters of the the active air spring prototype, the index (1) refers to the upper rolling piston, index 2 to the lower one.

static pressure $p(z = 0)$	14 bar(abs.)
outer radius r_{O1}	70 mm
rolling piston radius r_{P1}	(52.5 ± 3) mm
load-carrying area A_{L1}	$(11\,740 \pm 570)$ mm²
outer radius r_{L2}	63.5 mm
rolling piston radius r_{P2}	$(47 \mp 2{,}5)$ mm
load-carrying area A_{L2}	$(9\,545 \mp 340)$ mm²
total load-carrying area A_L	$(2\,195 \pm 910)$ mm²
axial force $F(z = 0)$	$(2\,850 \pm 1\,180)$ N
air spring volume V_0	2.8 l
maximal suspension travel z_{max}	±70 mm

When using a double bellows air spring with a ring-shaped load-carrying area

$$A_L = A_{L1} - A_{L2}\ , \qquad (6$$

even small changes of the rolling piston radii result in relative large area changes. To maximize the relative area change and the resulting change in the axial force, we use two actively adjustable rolling pistons. The actuator of the upper and lower piston move always in opposite directions. Furthermore, the power consumption is lower because the extending actuator is partly powered by the retracting one. No similar technologies are known to date. The air spring with an adjustable rolling piston by Meritor /12/, for example, cannot provide a defined axial force.

In order to show the functionality of the active air spring and to test it experimentally, we built a demonstrator of the air spring with two hydraulically adjustable rolling pistons (Figure 2). The most important parameters of the demonstrator are listed in the following Table 1.

In addition to component tests on a single axis testing machine by the manufacturer MTS, in which the force response of the strut $\underline{F}$ at specified compressions $\underline{z}$ is measured, we carry out hardware-in-the-loop (HiL) simulations with the active air spring.

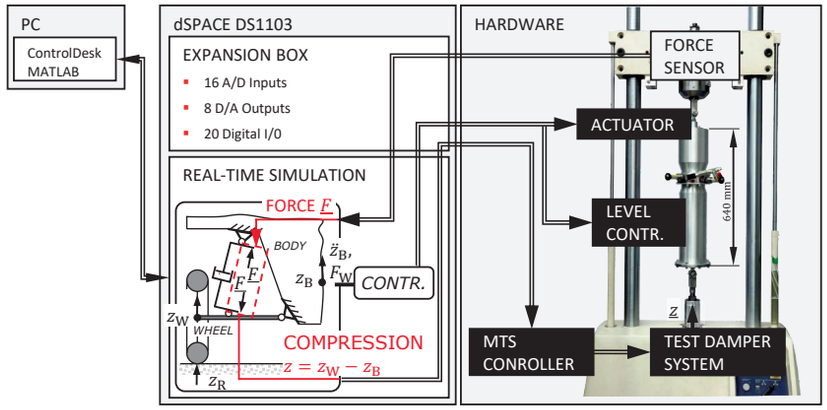

Figure 3: Simplified graphical diagram of the Hardware-in-the-Loop Simulation setup.

In these tests, the air spring is coupled with a virtual quarter car that is simulated in parallel in a real-time simulation environment by dSPACE. The basic structure and signal and power flows of the HiL experiments are shown in Figure 3 in a simplified form. The compression of the air spring z calculated in the real-time simulation is transmitted to the testing machine, which applies the compression $\underline{z}$. The measured axial force response $\underline{F}$ is fed back into the simulation (closed loop simulation). The controller is also implemented in the simulation model. The HiL tests offer the advantage that the interactions of the active air spring with the overall system can be investigated at an early stage of development. It is also easily possible to vary parameters of the virtual system and thus examine the active air spring in different test scenarios (different controllers, loads, excitations, etc.).

3 Modelling of the Overall System

The overall system of the active air spring, which consists of the air spring, the hydraulic actuator, the hydraulic power supply and the controller, is depicted in Figure 4. The hydraulic actuator consists of the two adjustable air spring rolling pistons and a common drive, which couples them. The adjustable rolling pistons can be modelled as single-acting cylinders. The coupling element is powered by a double-acting hydraulic cylinder. But it is also possible to use other types of actuators, for example an electromechanical actuator, to power the active air spring. The rolling piston radii r_{P1} and r_{P2} can be adjusted by a simple control of the position y_{Act} of the coupling element. To do so, we use a hydraulic control valve. The position of the valve spool is directly determined by the voltage U_V.

Air Spring We model the dynamic behaviour of the air spring physically using the conservation equations for mass and energy /13/. The thermal equation of state couples these two equations and the result is a non-linear differential equation system for the three thermodynamic state variables pressure, density and temperature of the

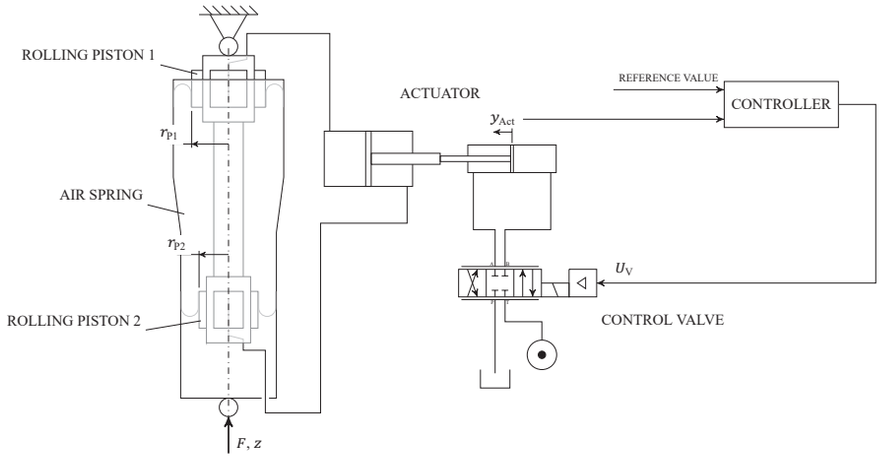

Figure 4: Schematic of the active air spring system and its components.

air in the enclosed air spring volume. The advantage of this formulation is, that one does not have to make any assumption for the change of state. The internal friction, which arises due to the deformation of the rolling bellows, can be represented as mechanic deformation energy and can be described as a series connection of springs and friction elements /6/. Measurements with the overall system have shown, however, that the stiffness of the air spring can be approximately described by a constant value of $10\,000\,\mathrm{N/m}$. For this reason, the air spring was simplified as a linear spring with the stiffness c as described in equation (4) for the control design. For a constant mass m for the air in the air spring, equation (4) can be simplified to

$$F = F_0 + cz + \Delta F_{\mathrm{Act}}\,, \tag{7}$$

with the axial actuating force $\Delta F_{\mathrm{Act}} = p_0\,\Delta A_{L0}$. The force ΔF_{Act} is, from a control engineering point of view, the output variable of the actuator "active air spring". It results from the effective piston radii $r_{\mathrm{P}\{1,\,2\}}$, which in turn depend on the position y_{Act} of the coupling element. Measurements show that these correlations can be regarded as simple linear factors K_{S} and K_{AS}. They are depicted on the right side of the block diagram shown in Figure 5. The feedback of the air spring pressure by the force acting on the rolling pistons, is neglected.

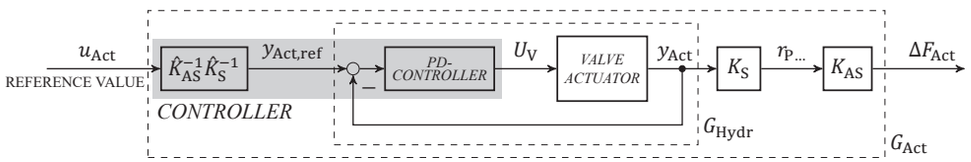

Figure 5: Block diagram of the controlled actuator.

Hydraulic Actuator Based on our measurements, the transfer function

$$G_{\mathrm{Act}}(s) = \frac{6\,097s + 5.226\cdot 10^5}{s^3 + 209.1s^2 + 2.391\cdot 10^4 s + 5.272\cdot 10^5} \tag{8}$$

for the hydraulic actuator was identified /14/. The approach of a system with one closed-loop zero and three poles is motivated by the assumption that the hydraulics can be described as an IT_2- or a PT_3-system, respectively, and the realization pole of the PD-controller in the relevant frequency range is negligible.

4 Model-based Chassis Control Design

In the following sections the ability of the presented actuator for being used within an active chassis control system is evaluated. For this purpose another control loop has to be designed, which aims to reduce the car body oscillations using the active air spring as actuator.

A good overview of the control of an active chassis can be found for example in /5, 15/. We use a linear H_2-optimal control because it enables a very systematic synthesis that leads to comparable results for system and control structure variations. Also, in this case the achievable control performance can be calculated analytically or – at least – it can be determined numerically without the need for simulations and does not depend on input scaling, as it would be the case for a non-linear control. As the HiL test stand allows only one active air spring to be examined, we limit our analysis to the control of a quarter car model.

This evaluation bases on the results presented in /14/ and extends these by considering a preview concept and deterministic road profiles like speed-bumps.

Model The model of the quarter car which is shown in Figure 6 is the basis for our control design. The control (actuating) input is u_{Act}, which is transformed into the actual actuating force ΔF_{Act} by the actuator with the transfer function G_{Act}. The disturbance input is the displacement of the road z_{R}.

The wheel load fluctuation $F_{\mathrm{W}} = c_{\mathrm{T}}\cdot(z_{\mathrm{R}} - z_{\mathrm{W}}) + d_{\mathrm{T}}\cdot(\dot{z}_{\mathrm{R}} - \dot{z}_{\mathrm{W}})$, the (car) body acceleration $\ddot{z}_{\mathrm{B}}$ and the compression $z = z_{\mathrm{W}} - z_{\mathrm{B}}$ are the relevant outputs for the evaluation of the control performance. Practical considerations aside, all model variables can be used as control (measured) outputs, i. e. controller inputs. All quantities are quantities of the linearised system, i. e. deviations around the operating point.

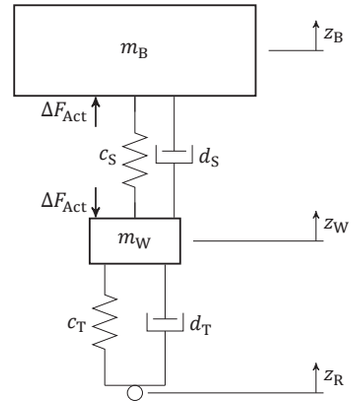

Figure 6: Quarter car model.

Table 2: Parameters of the quarter car.

body mass m_{B}	290 kg
wheel mass m_{W}	40 kg
suspension spring constant c_{S}	10 000 N/m ($\hat{=}c$)
suspension damping constant d_{S}	1 140 Ns/m
tire spring constant c_{T}	200 000 N/m
tire damping constant d_{T}	566 Ns/m

H_2-optimal controller synthesis for chassis control One possible interpretation of the H_2-norm of a stable system exists for stochastic signals. If the input **w** is normalized white noise, the H_2-norm is equal to the root of the square summed standard deviations $\sigma_{z,i}$ of the outputs **z** /16/,

$$\|\mathbf{z} \leftarrow \mathbf{w}\|_2 = \sqrt{\textstyle\sum_i \sigma_{z,i}^2}\,.$$

This interpretation fits to the modelling of road profiles as coloured noise, which is a frequently used in literature /5/. Based upon this, the concept of H_2-optimal controller synthesis is applied to the simplified, linearised model to demonstrate the principal relations and limits of the control.

The controller synthesis bases on the system shown in Figure 7. The transfer function

$$F_{\mathrm{R,LP}}(s) = \frac{2.1515 \cdot 10^{-2}\,\mathrm{m}}{6.4503 \cdot 10^{-5} \cdot s^3 + 2.0305 \cdot 10^{-2} \cdot s^2 + 1.6043 \cdot s + 1} \cdot \begin{bmatrix} 1 & s & s^2 \end{bmatrix}^{\mathrm{T}} \tag{9}$$

contains the road model as well as a second-order low pass filter with a cut-off frequency of 25 Hz to limit the observation to the low frequencies within the validity range of the quarter car model. Along with the road profile z_{R}, it outputs its first two derivatives. $F_{\mathrm{R,TP}}$ is appropriately scaled that the performance input n is equal to normalized white noise. The performance outputs for controller synthesis are the body acceleration $\ddot{z}_{\mathrm{B}}$, which is equivalent to the driving discomfort, the wheel load fluctuation F_{W}, which is equal to the driving safety, as well as the compression z and the actuating variable u_{Act} for assuring the functionality.

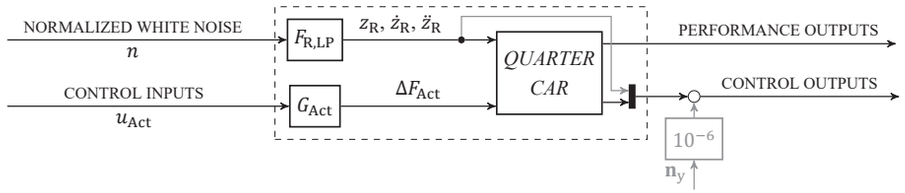

Figure 7: System for the controller design with preview.

The control outputs (measured variables) vary during the following analysis. In case of the preview control, they contain the signals z_{R}, $\dot{z}_{\mathrm{R}}$ and $\ddot{z}_{\mathrm{R}}$ (see below). If the function *systune* of the *Control System Toolbox* of MATLAB is used for the numerical optimization, the optimization problem can be formulated as

$$\min_{\mathbf{K}\in\mathcal{K}} \left(\|\ddot{z}_{\mathrm{B}} \leftarrow n\|_2^2 + \alpha_{\mathrm{F}}^2 \cdot \|F_{\mathrm{W}} \leftarrow n\|_2^2 \right)$$
$$\text{subject to} \quad \|z \leftarrow n\|_2 < \sigma_{\mathrm{z,max}}, \quad \|u_{\mathrm{Act}} \leftarrow n\|_2 < \sigma_{\mathrm{u_{Act},max}}\,. \tag{10}$$

The set $\mathcal{K}$ corresponds to a given structural constraint of the controller. For example, one can restrict the control to a static feedback. Varying α_{F} changes the weighting between the two optimization goals minimal body acceleration and minimal wheel load fluctuation. In this case, we limit the standard deviation of the compression $\sigma_{\mathrm{z,max}}$ to a a third of the maximum possible deflection and the standard deviation of actuator force $\sigma_{\mathrm{u_{Act},max}}$ to a third of the maximum actuator force.

In case of the "free optimization problem", i. e. if no structural constraints are given, one can calculate the optimal controller analytically for the objective function

$$V^2 = \|\ddot{z}_{\mathrm{B}} \leftarrow n\|_2^2 + \alpha_{\mathrm{F}}^2 \cdot \|F_{\mathrm{W}} \leftarrow n\|_2^2 + \alpha_{\mathrm{z}}^2 \cdot \|z \leftarrow n\|_2^2 + \alpha_{\mathrm{u_{Act}}}^2 \cdot \|u_{\mathrm{Act}} \leftarrow n\|_2^2 + V_{\mathrm{ny}}^2. \tag{11}$$

To fulfil all requirements for using this algorithm, a very small measurement noise V_{ny}^2, as indicated in Figure 7, must also be taken into account /16/. Chosen sufficiently small, it has a negligible effect on the results. The limitations of the compression and the actuator force are met by iteratively adapting the weighting factors α_{z} and $\alpha_{\mathrm{u_{Act}}}$.

The free H_2-optimal controllers are usually dynamic controllers of high order and therefore not suitable for practical use. However, they give the "reference" solution which can be used as a benchmark for simpler controllers.

Preview Concept In /14/ we showed, that there is a significant gap between the performance of the optimal, dynamic feedback and the performance which is achievable using static feedback. To close this gap, one could try to find simple dynamic controllers. Another way to improve the control performance is to apply preview concepts, which – of course – require suitable sensors.

The approach taken here follows /17/, where the preview sensor data is used to determine the displacement oft the road input z_{R} as well as its first two derivatives, $\dot{z}_{\mathrm{R}}$ and $\ddot{z}_{\mathrm{R}}$, at the current time.

It should be noted that the controllers also incorporate a weak integral action with regard to the compression. This is necessary to make the body follow the road in the long term, as comfort maximizing controllers tend to decouple body and wheel /15/. As the integrator gain is chosen rather small, it has only a minor influence on the presented results and hence, for sake of brevity, is not discussed in detail here.

Discussion The results for different controller configurations are depicted in the so-called conflict diagram, Figure 8. In this diagram, the body acceleration fluctuation $\sigma_{\ddot{z}_{\mathrm{B}}}$, which is equivalent to the "discomfort", is plotted over the dimensionless wheel-load fluctuation $\sigma_{F_{\mathrm{W}}}/F_{\mathrm{W,0}}$, the "driving safety", for a specific type of road and driving velocity. In our case, the results for a ride over an average German highway ("Bundesstraße") at a driving velocity of 100 km/h is shown. The results for other types of roads and different driving velocities are similar. The non-filled circle marks the performance values of a typical design of a passive suspension.The displayed lines are the Pareto lines for each controller and actuator configuration which mark the achievable maximal performance and can not be undercut.

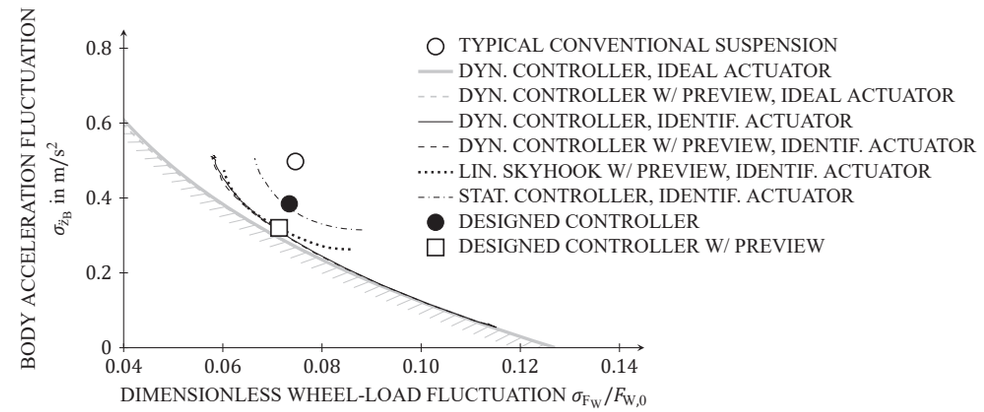

Figure 8: Pareto lines for different controller configurations, assuming an ideal actuator (grey) and the identified actuator (black).

The solid lines represent the optimal solutions of the free optimization problems with the objective function (11) if α_{F} varies (for increasing values for α_{F} one moves on the Pareto lines from the bottom right to the top left), using the variables z_{B}, $\dot{z}_{\mathrm{B}}$, z_{W} and $\dot{z}_{\mathrm{W}}$ (i. e. all mechanical states) as control output (measured variables). For the gray line an optimal actuator, i. e. $G_{\mathrm{Act}}(s) = 1$, is assumed, whereas the black line shows the result for the real actuator (8). As there are no structural constraints imposed, no linear controller can achieve values below the shown curves for equal limitations.

One can see that the actuator, due to its dynamics, increases – i. e. deteriorates – the achievable minimal wheel load fluctuation. That this effect worsens the wheel load fluctuation is reasonable, as its variance is primarily caused by the wheel's natural frequency of approximately 10 Hz. At this frequency the actuator is less effective due to its dynamics. On the contrary, the the body natural frequency of 1 Hz is far below the actuator's cut-off frequency. Consequently, the mitigation of the body acceleration is not effected by the actuator dynamics.

The black dash-dotted line represents static feedback of the variables z_{B}, $\dot{z}_{\mathrm{B}}$, z_{W} and $\dot{z}_{\mathrm{W}}$, the identified actuator considered. Also, like for the following designs, the controller coefficients are limited to the interval $[-1, 1]$, related to scaled variables (Forces: 1000 N, velocities: 0.1 m/s, distances: 0.01 m).

The already mentioned gap between this Pareto line and the one for the dynamic controller (i. e. the best possible solution) is apparent. However, the feedback of all mechanical states is still not realistic. For this reason, we only use the body velocity as feedback for first HiL simulations, i. e. $u_{\mathrm{Act}} = k_{\dot{z}_{\mathrm{B}}} \cdot \dot{z}_{\mathrm{B}}$. Optimization yields a parameter

value of approximately $k_{\dot{z}_B} = -1\,750\,\mathrm{Ns/m}$. Even with this simple structure, we are able to achieve values which are close to the Pareto line of the presented static "state feedback" structure. The achieved body acceleration is significantly smaller than the one for the passive suspension, which is marked by the non-filled circle in Figure 8.

The dashed lines are the solutions of the free optimization problem with preview, i. e. z_R, $\dot{z}_R$ and $\ddot{z}_R$ are included in the control outputs. This lines are hardly to see, as they are very close to theirs corresponding non-preview counterparts.

The black dotted line is the result for a simple, linear sky-hook controller (i. e. static feedback of body and wheel velocities) with preview. The preview variables z_R, $\dot{z}_R$ and $\ddot{z}_R$ are used with static gains as well, resulting in the static controller

$$u_{Act} = k_{\dot{z}_B} \cdot \dot{z}_B + k_{\dot{z}} \cdot \dot{z} + k_{z_R} \cdot z_R + k_{\dot{z}_R} \cdot \dot{z}_R + k_{\ddot{z}_R} \cdot \ddot{z}_R \,. \tag{12}$$

In contrast to the case with no preview, this line is very close to the Pareto line which can be achieved with a dynamic controller. I. e., the principal benefit of this preview concept is not to move the Pareto line into better regions but to make it achievable with simpler control structures. There is still an inherent limit for the achievable performance, which even a preview control cannot enhance. The reason for this is, that a preliminary action in order to achieve a better behaviour in reaction to a future excitation influences the present behaviour as well.

The filled square marks the controller used in the HiL experiments with the parameters $k_{\dot{z}_B} = -1\,750\,\mathrm{Ns/m}$, $k_{\dot{z}} = 0$, $k_{z_R} = -3\,860\,\mathrm{N/m}$, $k_{\dot{z}_R} = -1\,016\,\mathrm{Ns/m}$ and $k_{\ddot{z}_R} = -18.29\,\mathrm{Ns^2/m}$.

Conclusion Due to the dynamics of the actuator, certain trade-offs compared to an ideal reference have to be accepted. However, we can show that the actuator can achieve a significantly increase in the driving comfort, especially in the frequencies where oscillations cause motion sickness. Consequently, our active air spring could be used within an active chassis control system for minimizing motion sickness and maximizing driving comfort.

5 Actuator Validation in Hardware-in-the-Loop Experiments

The HiL set-up is sketched in Figure 3. The software-simulated system corresponds to the quarter car model shown in Figure 6 without the stiffness c_S, which is now generated by the real air spring. During the tests, the current deflection z is calculated from the system dynamics, the measured force $\underline{F}$ and the actual road excitation z_R and its derivative $\dot{z}_R$ and transmitted to the single axis testing machine, which then adjusts it. The force response of the active air spring is measured and used again as an input variable for the simulation model. The sampling time is 1 ms and we use a second-order Butterworth filter with a cut-off frequency of 170 Hz to smooth the force signal. In the relevant frequency range up to 20 Hz, the position-controlled testing machine can be described very well by a delay element of 10 ms, which coincides with known results /18/.

The influence of this delay and the filtering was examined in /14/ by comparing the calculated frequency responses of the overall systems comprising the ideal quarter car model and the HiL model, respectively. Only a very small effect within the relevant frequency range was observed.

For the experiments, we use the described form filter $F_{R,LP}$ to generate a virtual stochastic road profile for a time of 20 seconds. The profile is a periodical input for the HiL model. When the transient system response is faded out, we start the data acquisition and estimate the frequency response of the quarter car offline based on these data. The frequency responses shown in Figure 9b are those of the system including the road model $F_{R,LP}$, thus the input n, and the outputs wheel load fluctuation F_W and (car) body acceleration $\ddot{z}_B$.

Results, which were obtained using the described procedure, are shown in Figure 9. In Figure 9a the effect of a simple static feedback of the car body velocity (sky-hook control), $u_{Act} = k_{\dot{z}_B} \cdot \dot{z}_B$, with $k_{\dot{z}_B} = -1\,750\,\mathrm{Ns/m}$ is compared to the case without control. In Figure 9b the control with and without preview are compared. The solid lines illustrate the measured frequency response, while the dashed lines represent the frequency response calculated

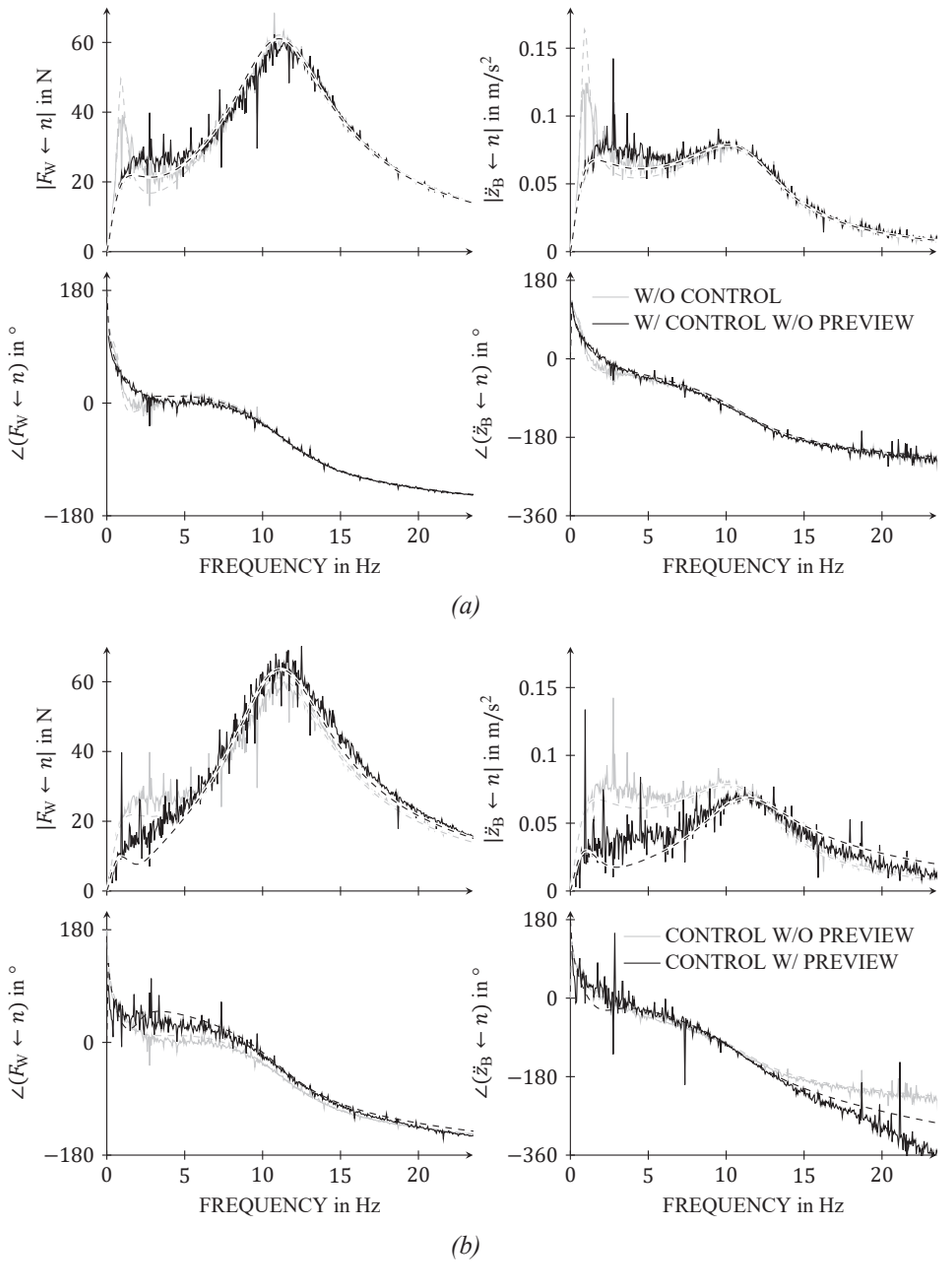

Figure 9: Comparison of measured (HiL-Simulation) and simulated frequency responses of the quarter car (solid line: measurement, dashed line: simulation) without and with static skyhook control (a) and without and with additional preview control (b).

based on the model. This calculation also takes into account the above mentioned effects (time delay, filtering) of the HiL test bench.

One can recognize that the models describe the behaviour with and without control qualitatively correct and quantitatively well. Only the increase in the range of the body's natural frequency is somewhat overestimated

in the case without control and somewhat underestimated in the controlled case. This shows the actually non-linear behaviour of the air spring, whose effective stiffness depends on the deflection amplitudes and velocities. The difference in the phase drop for frequencies over 15 Hz between the calculated and measured frequency response function for the body acceleration in the case of preview can be accounted to inaccuracies within the model of the hydraulic actuator. Apart from this, the model of the overall actuator can be considered validated for the operating point.

Especially in the frequency range around the body's natural frequency, which is the most relevant range for driving comfort and the main cause for motion sickness, the body accelerations are clearly reduced by the control with respect to the passive air spring ($k_{\dot{z}_B} = 0$) – and thus also clearly compared to a passive, conventional suspension not shown here. Using the preview concept, the accelerations are reduced even considerably more and over a wider frequency range.

As a second test case, driving over a speed-bump, a typical obstacle, is examined. The speed-bump is modelled as cosinus-shaped profile with a length of 1 m and a maximum height of 50 mm. The driving speed is 10 km/h. In the upper plot in Figure 10, the profile is plotted over the time.

Both the control with and without preview reduce the body movement clearly and prevent oscillations after the end of the speed-bump, as depicted in the second plot in Figure 10. However, the third plot shows that only the preview control is able to reduce the accelerations considerably in this case. This is reasonable, as the oscillation of the induced acceleration mainly lies in a frequency range where only the preview controller shows a clear reduction (see Figure 9).

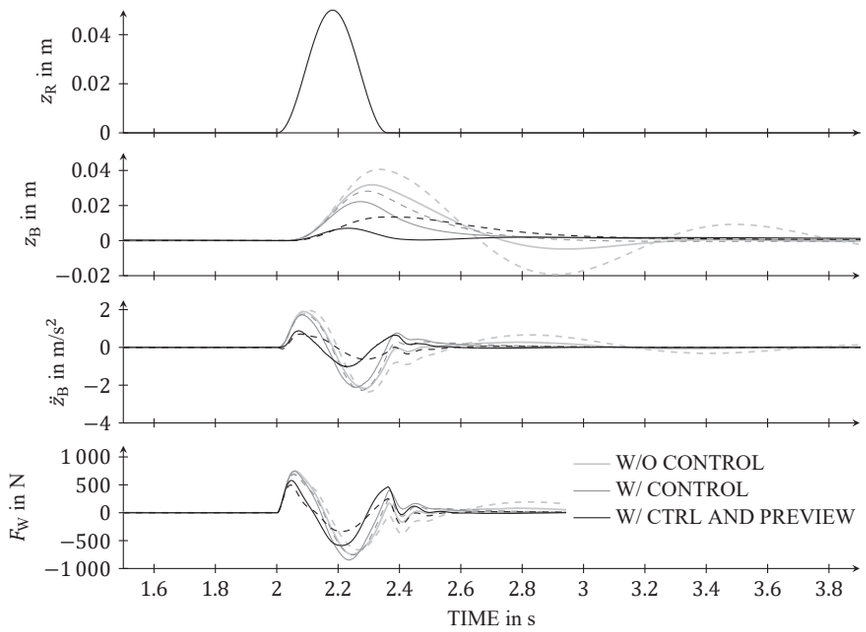

Figure 10: Comparison of measured (HiL-Simulation) and simulated time responses of the quarter car running over a speedbump at 10 km/h *(solid line: measurement, dashed line: simulation) for different controls.*

As in the case of stochastic excitation, the measured results fits the simulated ones qualitatively well, i. e. the relations (damping, principal shape of the curves) between the different configurations are correctly described, even if the overall damping is underestimated by the model. A possible work for the future is to examine the non-linear behaviour of the air spring more thoroughly to get a better understanding of its stiffness and damping.

6 Summary and Conclusion

We presented a new concept for an active suspension strut, an active air spring. The active air spring can manipulate the axial force independently of its deflection by changing its load-carrying area. Based on a linear model for the air spring and the actuator, a controller design for a quarter car was carried out. Hardware-in-the-Loop simulations with a prototype of the active air spring show its capability of reducing (car) body accelerations and thus improving the driving comfort for an exemplary ride over a typical German highway at 100 km/h. We were able to show, that the fluctuation of the body acceleration can be decreased with the active air spring and a skyhook controller by 23% and with a preview controller even by 36% at slightly improved ride safety. When riding over a cosine-shaped bump with a height of 50 mm at a driving velocity of 10 km/h, the maximum body acceleration was reduced by approx. 10% with the skyhook controller and by more than 50% with the preview controller at a slightly decreased wheel load fluctuation.

Summarized, by using the active air spring, a significantly increase in the driving comfort, especially in the frequencies where oscillations cause motion sickness, is achievable which could reduce its incidence.

As it is known that the oscillations at different frequencies have different impacts on the passengers /19/, one could incorporate a corresponding weighting filter into the synthesis procedure for optimizing the driving comfort, which emphases the low frequencies more. On the other hand, to enhance the behaviour with respect to single obstacles like a speed-bump, a weighting filter which amplifies high frequencies would be more adequate. To avoid this conflict, a double approach could be taken in which the normal controller is synthesized for a stochastic excitation considering the low frequencies more and when the sensors detect a single obstacle, a second parametrization is used.

It is also conceivable to use pneumatic instead of hydraulic damping. This can be easily realized by integrating a nozzle for dissipating the oscillation energy to the active air spring, which then becomes an active air spring damper. The active air spring damper combines the functions "load-carrying", "energy storing", "applying an actuating force" and "dissipating energy" in one component. The frequency-specific pneumatic damping /20/ prevents the strut from "becoming stiff" at higher excitations frequencies and the actuator would not need to work against the hydraulic damper.

7 Acknowledgements

The authors would like to thank the German Research Foundation (DFG) for funding this research within the Collaborative Research Centre (SFB) 805 "Control of Uncertainties in Load-Carrying Structures in Mechanical Engineering" (TU Darmstadt, speaker Prof. Dr.-Ing. Peter F. Pelz). Furthermore, the authors especially would like to thank the project cooperation partner Vibracoustic for supporting this project.

Nomenclature

The first column of the following table shows the symbols utilized for physical and mathematical quantities. The second column shows the meaning of each quantity. The dimension of each physical quantity is denoted in the third column, based on the generic quantities length (L), mass (M), time (T) and current (I).

Variable	*Description*	*Dimension*
$\alpha_{...}$	weighting factor (dimension depends on the weighted system path)	*
A_D	displacement area of the air spring	L^2
A_L	load-carrying area of the air spring	L^2
c	stiffness of the air spring	$M\,T^{-2}$
c_S	suspension spring constant	$M\,T^{-2}$
c_T	tire spring constant	$M\,T^{-2}$
d_S	suspension damping constant	$M\,T^{-1}$
d_T	tire damping constant	$M\,T^{-1}$
F	axial (air spring) force	$M\,L\,T^{-2}$
ΔF	(axial) actuator force	$M\,L\,T^{-2}$
F_0	static load	$M\,L\,T^{-2}$
$F_{R,LP}$	transfer function for generation of road profile	L
F_W	wheel-load	$M\,L\,T^{-2}$
G_{Act}	transfer function of the actuator	1
G_{Hydr}	transfer function of the hydraulic actuator	1
γ	isentropic constant	1
$k_{\dot{z}_B}$	control parameter for sky-hook control	$M\,T^{-1}$
m_B	mass of the (car) body	M
m_W	mass of the wheel	M
n	normalized white noise	1
n_y	measurement noise (dimensions depend on chosen control outputs)	*
ω	excitation frequency	T^{-1}
p	(air) pressure inside of the air spring	$M\,L^{-1}\,T^{-2}$
p_a	ambient pressure	$M\,L^{-1}\,T^{-2}$
r_O	outer radius of the air spring	L
r_P	rolling piston radius of the air spring	L
u_{Act}	actuator control value	L
U_V	control valve input voltage	$M\,L^2\,I\,T^{-3}$
V	quality criterion	1
V_0	volume of the air spring	L^3
y_{Act}	actuator displacement	L
z	compression of the air spring	L
z_B	displacement of the (car) body	L
$\ddot{z}_B$	(car) body acceleration	$L\,T^{-2}$
z_R	displacement of the road input	L
z_W	displacement of the wheel	L

References

/1/ D. Heinrichs. “Autonomes Fahren und Stadtstruktur”. In: *Autonomes Fahren: Technische, rechtliche und gesellschaftliche Aspekte*. Ed. by M. Maurer et al. Berlin, Heidelberg: Springer Berlin Heidelberg, 2015, pp. 219–239.

/2/ M. Sivak and B. Schoettle. *Motion Sickness in Self-Driving Vehicles*. Report. Transportation Research Institute, University of Michigan, 2015.

/3/ C. Diels and J. E. Bos. “Self-driving carsickness”. In: *Appl Ergon* 53 Pt B, 2016, pp. 374–82.

/4/ H. Winner and W. Wachenfeld. “Auswirkungen des autonomen Fahrens auf das Fahrzeugkonzept”. In: *Autonomes Fahren: Technische, rechtliche und gesellschaftliche Aspekte*. Ed. by M. Maurer et al. Berlin, Heidelberg: Springer Berlin Heidelberg, 2015, pp. 265–285.

/5/ M. Mitschke and H. Wallentowitz. *Dynamik der Kraftfahrzeuge*. Wiesbaden: Springer Vieweg, 2014.

/6/ P. F. Pelz and M. Mess. “Luftfederung und Luftdämpfung im Spannungsfeld Komfort, Dynamik und Sicherheit”. In: *ATZ* 109.03, 2007.

/7/ T. Bedarff and P. F. Pelz. “Entwicklung und Untersuchung eines innovativen, aktiven Federungssystems”. In: *VDI Berichte 2138*. 2011, pp. 283–294.

/8/ B. Heißing, M. Ersoy, and S. Gies. *Fahrwerkhandbuch*. Wiesbaden: Vieweg, 2011.

/9/ T. Bedarff and P. F. Pelz. “Schwingungsminderung durch ein aktives hydro-pneumatisches Feder-Dämpfer-System”. In: *VDI Berichte 2164*. 2011, pp. 93–106.

/10/ P. Hedrich, M. Johe, and P. F. Pelz. “Design and Realization of an Adjustable Fluid Powered Piston for an Active Air Spring”. In: *10th IFK, Dresden*. 2016, pp. 571–582.

/11/ P. Hedrich, M. Johe, and P. F. Pelz. *Patent DE102015120011A1*. May 18, 2017.

/12/ J. T. Peterson. *Patent EP2230108A2*. Sept. 22, 2010.

/13/ P. F. Pelz. “Beschreibung von pneumatischen Dämpfungssystemen mit dimensionsanalytischen Methoden”. In: *VDI Berichte 2003*. 2007, pp. 289–304.

/14/ P. Hedrich, E. Lenz, and P. F. Pelz. “Modellbildung, Regelung und experimentelle Untersuchung einer aktiven Luftfederung in einer Hardware-in-the-Loop-Simulationsumgebung”. In: *VDI Berichte 2295*. 2017, pp. 447–460.

/15/ R. H. Streiter. “Entwicklung und Realisierung eines analytischen Regelkonzeptes für eine aktive Federung”. D 83. PhD thesis. Technische Universität Berlin, 1996.

/16/ K. Zhou. *Essential of Robust Control*. Upper Saddle River, NJ: Prentice Hall, 1998.

/17/ A. Schindler. “Neue Konzeption und erstmalige Realisierung eines aktiven Fahrwerks mit Preview-Strategie”. PhD thesis. Universität Karlsruhe, 2009.

/18/ D. C. Batterbee et al. “Hardware-in-the-loop simulation of a vibration isolator incorporating magnetorheological fluid damping”. In: *ECCOMAS*. 2005.

/19/ Verein Deutscher Ingenieure. *Einwirkung mechanischer Schwingungen auf den Menschen - Blatt 1: Ganzkörper-Schwingungen*. Norm. Sept. 2002.

/20/ P. F. Pelz and R. Sonnenburg. “Bestimmung komfortoptimaler Designparameter eines Luft-Feder-Dämpfers im Fahrzeugmodell”. In: *VDI Berichte 1846*. 2004, pp. 527–542.